Dyes and Pigments 187 (2021) 109079

Contents lists available at ScienceDirect

Dyes and Pigments

journal homepage: http://www.elsevier.com/locate/dyepig

Marked effects of azulenyl *vs.* naphthyl groups on donor-π-acceptor-π-donor small molecules for organic photovoltaic cells

Lin Yang [a,b,1], Youqin Zhu [c,1], Jueshan Liu [a], Yao Chen [a], Jianglin Wu [a], Zhenguo Pang [a], Zhiyun Lu [a], Suling Zhao [c,**], Yan Huang [a,*]

[a] Key Laboratory of Green Chemistry and Technology, Ministry of Education, College of Chemistry, Sichuan University, Chengdu, 610064, PR China
[b] School of Pharmaceutical Sciences, Southwest Medical University, Luzhou, Sichuan, 646000, PR China
[c] Key Laboratory of Luminescence and Optical Information, Ministry of Education, Institute of Optoelectronics Technology, Beijing Jiaotong University, Beijing, 100044, PR China

ARTICLE INFO

Keywords:
Azulene
Guaiazulene
Naphthalene
D-A conjugated semiconductors
Organic photovoltaics

ABSTRACT

Although the unique electronic and optical properties of azulene, the azulene-containing organic photovoltaic (OPV) materials have sporadically reported. Here, eight donor-π-acceptor-π-donor conjugated OPV materials entailing guaiazulene or naphthalene as electron donor unit were synthesized and characterized. The azulenyl and naphthyl groups have significant influences on their molecular properties and photovoltaic performances. Compared to naphthalene derivatives, azulene derivatives exhibit red-shifted and wider absorption spectra. However, naphthalene derivatives exhibit much deeper highest occupied molecular orbital (HOMO) energy levels, higher hole mobility and better film morphology, remarkably resulting in approximately 2–4 times higher photovoltaic efficiencies than azulene derivatives.

1. Introduction

Donor-acceptor (D-A) conjugated organic semiconductive materials, employed as photoactive layers in bulk heterojunction (BHJ) organic photovoltaic cells (OPVs), have been extensively studied due to their advantages of rich structural diversity and easily tunable optical absorption properties, energy levels, solubility, planarity etc. [1–4] Typically, the prevalent strategy of constructing D-A conjugated photoactive materials is to select appropriate D or A units, connect D and A units in different ways (such as D-A, D-A-D, A-D-A, etc.) and modify the side chains [5–7]. The considerable efforts on developing D-A conjugated photoactive materials have pushed the impressive power conversion efficiencies (PCEs) of OPVs to over 18% [8].

Azulene, also known as blue hydrocarbon, is an aromatic bicyclic 10 π-electron isomer of naphthalene (shown in Fig. 1). Azulene shows a special non-alternant aromatic hydrocarbon structure with an electron-deficient seven-membered ring and an electron-rich five-membered ring [9,10], resulting in different properties from naphthalene. For example, azulene has a large dipole moment of about 1.08 D [9,10], while that of naphthalene is 0 D. Azulene shows beautiful blue color while naphthalene is colorless [11,12], due to the small energy gap of azulene caused by its non-mirror-related frontier orbital geometry [10,13]. So it is reported that azulene derivatives have much lower energy gaps than naphthalene derivatives [14]. Due to the unique electronic and optical properties of azulene, azulene derivatives have been gradually considered to be promising candidates in organic electronic and photovoltaic devices in recent years [10,15], including organic field effect transistors (OFETs) [16–19], OPVs [13,20–23], dye-sensitized solar cells (DSSCs) [12,24] and perovskite solar cells [25,26], etc.

Up to now, azulene derivatives employed as OPV materials have sporadically reported. In 2014, Emrick et al. synthesized novel azulene-substituted methacrylate polymers (PATSB1-3, shown in Fig. 2) and examined their role as interlayer in BHJ OPVs [22]. In 2015, Imahori et al. designed four D¬A alternating polymers (PAzDPP and PAzBT1¬3, shown in Fig. 2) containing azulene as a donor unit and diketopyrrolopyrrole (DPP) or 2,1,3-benzothiadiazole (BT) unit as an acceptor unit and investigated their optical and photovoltaic properties [21]. Shortly afterwards, Zhang et al. reported three new alternating

* Corresponding author.
** Corresponding author.
E-mail addresses: slzhao@bjtu.edu.cn (S. Zhao), huangyan@scu.edu.cn (Y. Huang).
[1] These authors contributed equally.

https://doi.org/10.1016/j.dyepig.2020.109079
Received 1 September 2020; Received in revised form 12 November 2020; Accepted 6 December 2020
Available online 5 January 2021

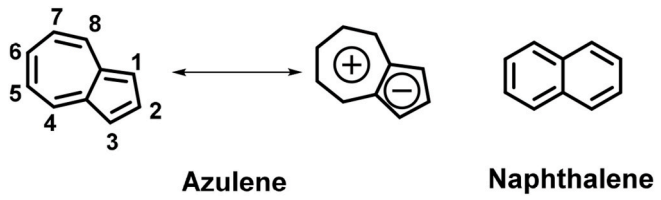

Fig. 1. Chemical structures of azulene and naphthalene.

dithienyldiketopyrrolopyrrole-azulene conjugated polymers (DPPA1-3, shown in Fig. 2) by varying the linking positions of azulene and investigated their OFET and OPV performances [20]. In 2018, Gao et al. designed two conjugated polymers (P(TBAzDI-TPD) and P(TBAzDI-TFB), shown in Fig. 2) by incorporation of 2,6-connected azulene units into the backbone, exhibiting relatively high OFET and OPV performances [13]. Aside from these azulene-containing OPV polymers, only our group reported two azulene-containing small molecules for OPVs and obtained a relatively highest PCE of 2.23% among the current azulene-containing OPV materials [23]. It can be seen that the evaluation of azulene group in OPV materials remains scarce. Moreover, to our knowledge, there are no literatures to compare the effects of azulene and naphthalene groups on the properties and photovoltaic performances of OPV materials. Hence, we aim to develop novel azulene-containing OPV materials and investigate the effects of azulene and naphthalene groups on the properties and photovoltaic performances of their derivatives.

In this paper, guaiazulene, one of azulene derivatives, was chosen as the electron-donating group because of its low-cost and good solubility [17]. Therefore, eight D-A-D conjugated azulene and naphthalene derivatives (shown in Scheme 1), containing guaiazulene or naphthalene as electron-donating moiety and BT, DPP, isoindigo (IID), or thienothiophene (TT) as electron-withdrawing moiety, were synthesized and employed as the electron donor materials in OPVs. The effects of azulene and naphthalene groups on the molecular properties and photovoltaic performances were researched.

2. Experimental section

2.1. Measurements

^{1}H (400 MHz) and ^{13}C (100 MHz) nuclear magnetic resonance (NMR) spectra were recorded on a Bruker AVANCE III HD 400 M NMR spectrometer with tetramethylsilane as internal standard. Elemental analyses were measured with a Flash EA 1112 Organic Element Analyzer. Absorption spectra in chloroform solution (1×10^{-5} mol L^{-1}) and thin films were measured with a UV 2600 UV–Vis scanning spectrophotometer. The thin film samples were fabricated by spin-casting the chloroform solution of target compound (5 mg mL^{-1}) on quartz substrates (1500 rpm, 30 s). The thin film samples of Az-DPP and Na-IID were fabricated by spin-casting their chloroform solutions with a concentration of 2.5 mg mL^{-1} due to their limited solubility while that of Na-DPP wasn't prepared because of its rather poor solubility in chloroform (<0.5 mg mL^{-1}).

Cyclic voltammetry measurements were performed on a LK 2010 electrochemical work station with a three-electrode cell in 0.10 mol L^{-1} tetrabutylammonium perchlorate in anhydrous dichloromethane solution (the concentration of target compound is 5×10^{-4} mol L^{-1}). The three-electrode cell uses a Pt disk as working electrode, a Pt wire as counter electrode and a $Ag/AgNO_3$ (0.1 mol L^{-1} in acetonitrile) as reference electrode (ferrocenium/ferrocene redox couple as the internal potential reference). All measurements were carried out at room temperature at N_2 atmosphere with a scan rate of 50 mV s^{-1}.

Atomic force microscopy (AFM) measurements were measured with a MFP 3D Asylum Research atomic force microscope. Samples were prepared by spin-casting the chloroform solution of target compound [6,6]:-phenyl-C71butyric acid methyl ester ($PC_{71}BM$, 18 mg mL^{-1}, 1:5 in wt%) on glass substrate (2000 rpm, 50 s). The transmission electron microscopy (TEM) investigation was performed on a JEM-2100F field emission transmission electron microscope. Samples were prepared by spin-casting the chloroform solution of target compound:$PC_{71}BM$ (18 mg mL^{-1}, 1:5 in wt%) on poly(3,4-ethylenedioxythiophene)-poly (styrenesulfonate) (PEDOT:PSS)-coated glass substrate, then floating the film on water surface, and transferring to copper grids.

2.2. Device preparation

Photovoltaic devices were fabricated with a layered structure of

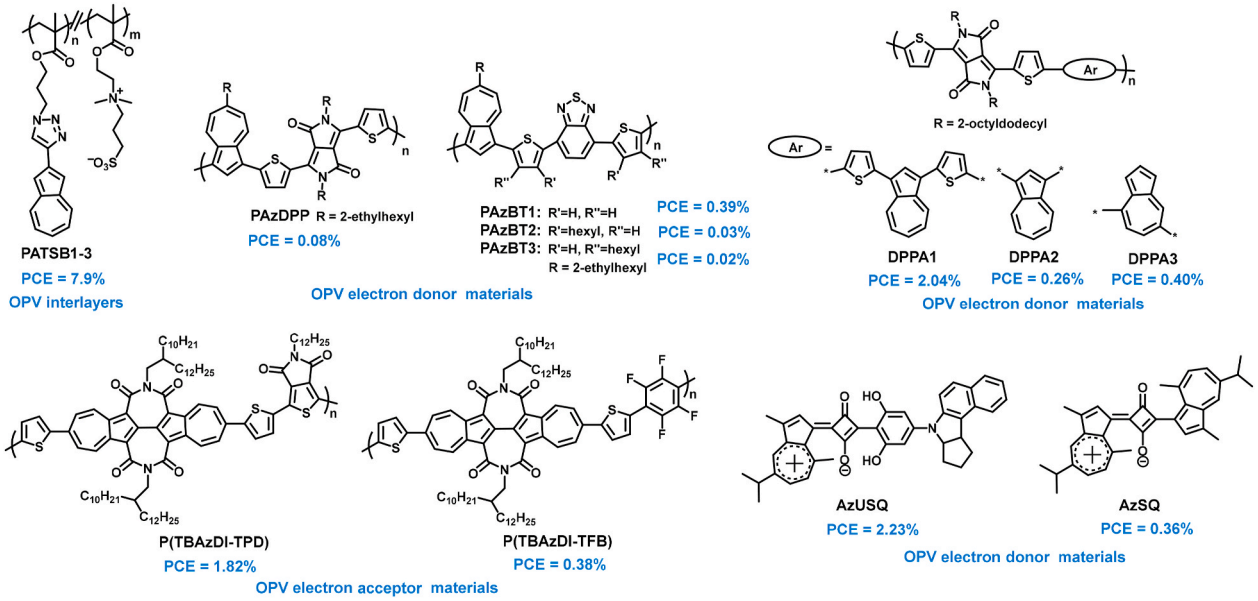

Fig. 2. Chemical structures of azulene-containing OPV materials [13,20–23].

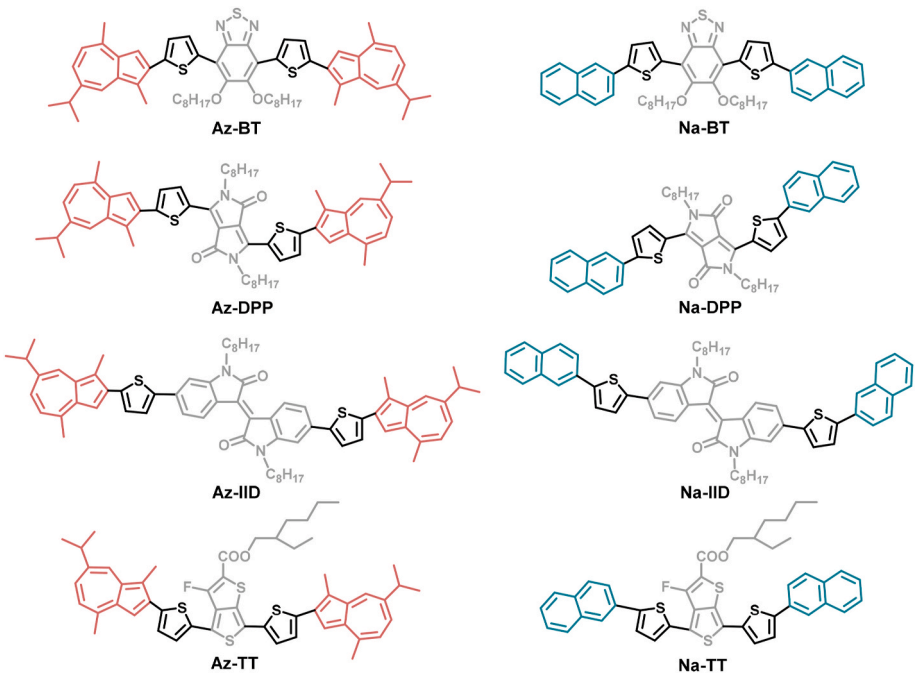

Scheme 1. Chemical structures of the target compounds.

glass/ITO/MoO_3 (8 nm)/target compound:$PC_{71}BM$ (wt/wt, 65 nm)/poly [(9,9-bis(3'-(*N*,*N*-dimethylamino)propyl)-2,7- fluorene)-alt-2,7-(9,9-dioctylfluorene)] (PFN, 5 nm)/Al (100 nm). The ITO-coated glass substrates (sheet resistance = 15 Ω sq^{-1}) were cleaned through sequential sonication in detergent, deionized water, acetone and ethanol for 10 min each, and finally blow-dried by high purity N_2. The substrates were expose to UV-ozone for 5 min, then immediately transferred into a high vacuum chamber ($<3 \times 10^{-4}$ Pa) to deposit MoO_3 layer (8 nm, 0.5

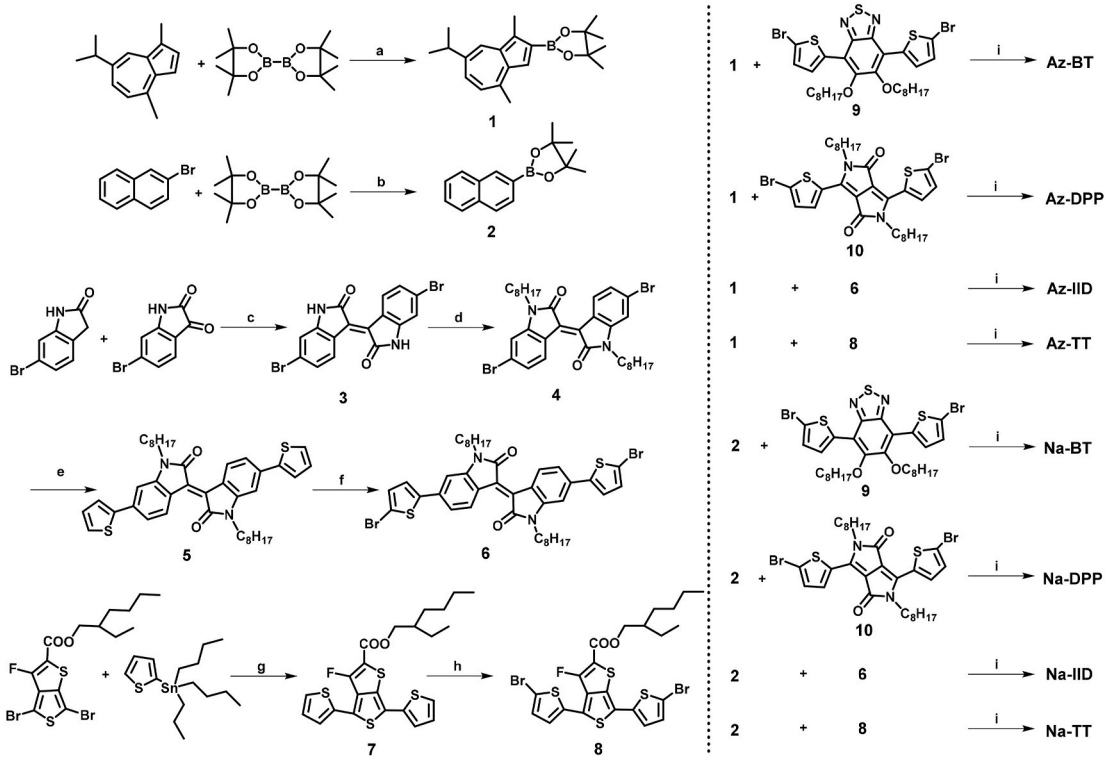

Scheme 2. Synthetic routes of the intermediates and target compounds. Reagents/conditions: a) 2,2′-bipyridine (7% eq.), chloro(1,5-cyclooctadiene)iridium(I) dimer (2.5% eq.), anhydrous cyclohexane, 80 °C, 20 h, 24%; b) $PdCl_2(dppf)_2$ (10% eq.), potassium acetate, anhydrous 1,4-dioxane, 80 °C, 10 h, 49%; c) acetic acid, concentrated HCl, reflux, 12 h, 87%; d) *n*-Bromooctane, potassium carbonate, DMF, 100 °C, 12 h, 29%; e) 2-tributylstannylthiophene, $Pd_2(dba)_3$ (2% eq.), P(*o*-tol)$_3$ (16% eq.), anhydrous toluene, reflux, 10 h, 90%; f) *N*-bromosuccinimide (NBS), tetrahydrofuran, r.t., 4 h; g) $Pd_2(dba)_3$ (2% eq.), P(*o*-tol)$_3$ (16% eq.), anhydrous toluene, reflux, 11 h, 87%; h) NBS, DMF, r.t., 2 h, 50%; i) $Pd(pph_3)_4$ (6% eq.), sodium carbonate, toluene:ethanol:water (1:1:1.5, v/v/v), 90 °C, 12 h, 79% (Az-BT), 48% (Az-DPP), 45% (Az-IID), 77% (Az-TT), 81% (Na-BT), 58% (Na-DPP), 65% (Na-IID), 81% (Na-TT).

Å s^{-1}). Subsequently, the photoactive layers were fabricated by spin-casting the chloroform solution of target compound:$PC_{71}BM$ (18 mg mL^{-1}, 1:5 in wt%, 2000 rpm, 50 s) in a N_2-filling glove box at 25 °C. Then the PFN methanol solution (2 mg mL^{-1}, with 2 μL mL^{-1} acetic acid) was spin-casted on the photoactive layers. Then the substrates were loaded into a vacuum chamber (<3 × 10^{-4} Pa) to finish the deposition of Al (100 nm, 1.5 Å s^{-1}). Deposition rate and film thickness were in situ monitored using a quartz crystal oscillator mounted to the substrate holder. The active area of cells was 3.8 mm^2. Several batches of devices (4 cells per batch) were fabricated and tested. The current density-voltage (*J-V*) curves under illumination were measured using an Abet solar simulator with a Keithley 4200 source measurement unit under AM 1.5G illumination (100 mW cm^{-2}) after spectral mismatch correction under an ambient atmosphere at 25 °C. External quantum efficiency (EQE) curves were performed in air atmosphere using a QE/IPCE Measurements Solar Cell Scan 100 (ZOLIX) system.

Hole-only devices were fabricated with a structure of ITO/MoO_3 (8 nm)/active layer/Au (100 nm). The dark *J-V* characteristics were measured and fitted the results using the space charge limited current (SCLC) model [27,28]. The current density (*J*) is given by

$$J = \frac{9}{8}\varepsilon_0\varepsilon_r\mu\frac{V^2}{L^3}$$

Where ε_0 is the permittivity of free-space, ε_r is the relative dielectric constant of the active layer, μ is the charge carrier mobility, and *L* is the thickness of the active layers.

2.3. Synthesis

The synthetic routes are outlined in Scheme 2. Compounds **1**–**8** were prepared according to the procedures described in the literatures [29–32]. Compounds **9**, **10** were purchased from Beijing HWRK Chem. The other chemicals, reagents, solvents were used as received from the suppliers except as specifically mentioned.

2.3.1. 2-(7-Isopropyl-1,4-dimethylazulen-2-yl)-4,4,5,5-tetramethyl-1,3,2-dioxaborolane (1) [29]

Guaiazulene (4.00 g, 20.00 mmol), bis(pinacolato)diboron (5.63 g, 22.00 mmol), 2,2′-bipyridyl (0.22 g, 1.40 mmol, 7% eq.) and chloro(1,5-cyclooctadiene)iridium(I) dimer (0.34 g, 0.5 mmol, 2.5% eq.) were added to anhydrous cyclohexane (60 mL). After argon gas was bubbled into the mixture for 10 min, the mixture was heated at 80 °C for 20 h, and filtered. The filtrate was concentrated under reduced pressure, and the crude product was purified by silica gel column chromatography (neutral alumina, *n*-hexane) to afford **1** (1.56 g, 24%) as blue-black solid and the recovery of guaiazulene is 45% (1.80 g). ^{1}H NMR (400 MHz, $CDCl_3$, ppm) δ 8.23 (d, J = 2.0 Hz, 1H, ArH), 7.60 (s, 1H, ArH), 7.38 (dd, J = 10.8 Hz, 1.6 Hz, 1H, ArH), 6.93 (d, J = 10.8 Hz, 1H, ArH), 3.10-3.00 (m, 1H, CH), 2.82 (s, 3H, CH_3), 2.81 (s, 3H, CH_3), 1.40 (s, 12H, CH_3), 1.35 (d, J = 6.8 Hz, 6H, CH_3).

2.3.2. 4,4,5,5-Tetramethyl-2-(naphthalen-2-yl)-1,3,2-dioxaborolane (2) [30]

2-Bromonaphthalene (2.00 g, 9.70 mmol), bis(pinacolato)diboron (3.06 g, 12.10 mmol), $PdCl_2$(dppf)$_2$ (0.71 g, 0.97 mmol, 10% eq.), and anhydrous potassium acetate (2.86 g, 29.10 mmol) were added to anhydrous 1,4-dioxane (60 mL). After argon gas was bubbled into the mixture for 10 min, the mixture was heated at 80 °C for 10 h, and filtered. The filtrate was concentrated under reduced pressure, and the crude product was purified by silica gel column chromatography (neutral alumina, *n*-hexane) to afford **2** (1.20 g, 49%) as white solid. ^{1}H NMR (400 MHz, $CDCl_3$, ppm) δ 8.37 (s, 1H, ArH), 7.88 (dd, J = 7.6 Hz, 1.6 Hz, 1H, ArH), 7.84-7.81 (m, 3H, ArH), 7.53-7.45 (m, 2H, ArH), 1.39 (s, 12H, CH_3). ^{13}C NMR (100 MHz, $CDCl_3$, ppm) δ 136.4, 135.2,133.0, 130.6, 128.8, 127.9, 127.2, 126.0, 110.2, 84.1, 25.1.

2.3.3. (E)-6,6′-dibromo-[3,3′-biindolinylidene]-2,2′-dione (3) [31]

6-Bromo-1,3-dihydro-2*H*-indol-2-one (2.00 g, 9.43 mmol) and 6-bromoindoline-2,3-dione (2.13 g, 9.43 mmol) were added to acetic acid (60 mL), then 0.4 mL concentrated HCl was added. The mixture was refluxed for 12 h. After cooled to room temperature, the brown precipitate was filtered, washed with water and dried to afford **3** (3.45 g, 87%) as brown solid. ^{1}H NMR (400 MHz, DMSO-d_6, ppm) δ 11.11 (s, 2H, NH), 8.99 (d, J = 8.8 Hz, 2H, ArH), 7.19 (dd, J = 8.8 Hz, 2.0 Hz, 2H, ArH), 7.00 (d, J = 2.0 Hz, 2H, ArH). ^{13}C NMR (100 MHz, DMSO-d_6, ppm) δ 168.9, 145.5, 132.7, 130.9, 125.7, 124.0, 120.8, 112.4.

2.3.4. (E)-6,6′-dibromo-1,1′-dioctyl-[3,3′-biindolinylidene]-2,2′-dione (4) [31]

3 (3.00 g, 7.14 mmol), potassium carbonate (4.93 g, 35.7 mmol), and *n*-bromooctane (3.03 g, 15.7 mmol) were added to *N*,*N*-dimethylformamide (DMF, 100 mL) under Ar atmosphere. The mixture was heated at 100 °C for 12 h, then poured into water, and filtered to obtain black solid. The solid was dissolved in 70 mL dichloromethane, and 400 mL petroleum ether was added dropwise to precipitate red solid, then filtered to give **4** (1.32 g, 29%) as red solid. ^{1}H NMR (400 MHz, $CDCl_3$, ppm) δ 9.07 (d, J = 8.8 Hz, 2H, ArH), 7.17 (dd, J = 8.8 Hz, 2.0 Hz, 2H, ArH), 6.92 (d, J = 1.6 Hz, 2H, ArH), 3.73 (t, J = 7.2 Hz, 4H, CH_2), 1.72-1.64 (m, 4H, CH_2), 1.42-1.21 (m, 20H, CH_2), 0.87 (t, J = 6.8 Hz, 6H, CH_3).

2.3.5. (E)-1,1′-dioctyl-6,6′-di(thiophen-2-yl)-[3,3′-biindolinylidene]-2,2′-dione (5) [31]

4 (1.00 g, 1.55 mmol), 2-tributylstannylthiophene (1.74 g, 4.65 mmol), Pd_2(dba)$_3$ (57 mg, 0.06 mmol, 2% eq.), and P(*o*-tol)$_3$ (90 mg, 0.29 mmol, 16 eq.) were added to anhydrous toluene (50 mL) under Ar atmosphere. The mixture was refluxed for 10 h, and the reaction was monitored by thin layer chromatography (TLC). After reaction, the solvent was concentrated under reduced pressure and the residue was purified by silica gel column chromatography (petroleum ether: dichloromethane = 2:1) to afford **5** (0.90 g, 90%) as brown solid. ^{1}H NMR (400 MHz, $CDCl_3$, ppm) δ 9.18 (d, J = 8.4 Hz, 2H, ArH), 7.43 (dd, J = 3.6 Hz, 0.8 Hz, 2H, ArH), 7.36 (dd, J = 4.8 Hz, 0.8 Hz, 2H, ArH), 7.30 (dd, J = 8.4 Hz, 1.6 Hz, 2H, ArH), 7.13 (t, J = 4.4 Hz, 2H, ArH), 6.98 (d, J = 1.6 Hz, 2H, ArH), 3.82 (t, J = 7.2 Hz, 4H, CH_2), 1.78-1.70 (m, 4H, CH_2), 1.46-1.24 (m, 20H, CH_2), 0.87 (t, J = 7.2 Hz, 6H, CH_3).

2.3.6. (E)-6,6′-bis(5-bromothiophen-2-yl)-1,1′-dioctyl-[3,3′-biindolinylidene]-2,2′-dione (6) [31]

5 (500 mg, 0.77 mmol) was dissolved in 50 mL THF, then NBS (300 mg, 1.68 mmol) was added. The mixture was stirred at 21 °C for 4 h in the dark. When the mixture was poured into 200 mL water, the brownish-black solid was precipitated immediately, and filtered to afford **6** (0.40 g, 64%), which was taken directly to the next step. ^{1}H NMR (400 MHz, $CDCl_3$, ppm) δ 9.17 (d, J = 8.4 Hz, 2H, ArH), 7.19 (dd, J = 8.0 Hz, 1.6 Hz, 2H, ArH), 7.17 (d, J = 4.0 Hz, 2H, ArH), 7.07 (d, J = 3.6 Hz, 2H, ArH), 6.87 (d, J = 1.6 Hz, 2H, ArH), 3.80 (t, J = 7.2 Hz, 4H, CH_2), 1.76-1.68 (m, 4H, CH_2), 1.45-1.26 (m, 20H, CH_2), 0.85 (t, J = 7.2 Hz, 6H, CH_3).

2.3.7. 2-Ethylhexyl-3-fluoro-4,6-di(thiophen-2-yl)thieno[3,4-b]thiophene-2-carboxylate (7) [32]

2-Ethylhexyl-4,6-dibromo-3-fluorothieno[3,4-*b*]thiophene-2-carboxylate (1.00 g, 2.11 mmol), 2-tributylstannylthiophene (1.96 g, 5.25 mmol), Pd_2(dba)$_3$ (38 mg, 2% eq.) and P(*o*-tol)$_3$ (102 mg, 16% eq.) were added to anhydrous toluene (40 mL) under Ar atmosphere. The mixture was refluxed for 11 h and the reaction was monitored by thin layer chromatography. After reaction, the solvent was concentrated under reduced pressure and the residue was purified by silica gel column chromatography (petroleum ether:dichloromethane = 5:1) to afford **7** (0.87 g, 87%) as yellow-orange solid. ^{1}H NMR (400 MHz, $CDCl_3$, ppm) δ 7.42 (dd, J = 3.6 Hz, 1.2 Hz, 1H, ArH), 7.38 (dd, J = 7.6 Hz, 0.8 Hz, 1H,

ArH), 7.36 (dd, J = 7.6 Hz, 0.8 Hz, 1H, ArH), 7.27-7.26 (m, 1H, ArH), 7.13-7.10 (m, 2H, ArH), 4.26 (dd, J = 5.6 Hz, 1.6 Hz, 2H, CH_2), 1.75-1.69 (m, 1H, CH), 1.48-1.28 (m, 8H, CH_2), 0.97-0.92 (m, 6H, CH_3).

2.3.8. 2-Ethylhexyl-4,6-bis(5-bromothiophen-2-yl)-3-fluorothieno[3,4-b] thiophene-2-carboxylate (8) [32]

7 (0.95 g, 2.00 mmol) was dissolved in DMF (10 mL). The mixture was stirred for 30 min in ice bath. Then a solution of NBS (0.78 g, 4.39 mmol) in DMF (20 mL) was added dropwise. The mixture was reacted at room temperature for 2 h. When the reaction solution was poured into water, the orange-red solid was precipitated, and filtered, recrystallized to afford **8** (0.66 g, 50%). ^{1}H NMR (400 MHz, $CDCl_3$, ppm) δ 7.14 (dd, J = 4.0 Hz, 0.8 Hz, 1H, ArH), 7.06 (dd, J = 3.6 Hz, 1.6 Hz, 2H, ArH), 6.98 (d, J = 4.0 Hz, 1H, ArH), 4.26 (dd, J = 5.6 Hz, 1.2 Hz, 2H, CH_2), 1.74-1.68 (m, 1H, CH), 1.49-1.33 (m, 8H, CH_2), 0.97-0.90 (m, 6H, CH_3).

2.3.9. Procedure for the synthesis of target compounds

$PdCl_2$ (200 mg, 1.12 mmol) and triphenylphosphine (1.48 g, 5.60 mmol) were added to degassed dimethyl sulfoxide (DMSO, 32 mL) under anhydrous condition in the dark, and the mixture was heated at 140 °C. When the reaction solution changed from a turbid solution to an orange-yellow clear one, the reaction mixture was cooled slightly and hydrazine hydrate (0.4 mL) was injected with a syringe in the dark to precipitate pale yellow solid. The reaction mixture was cooled to room temperature, filtered, washed with ethanol and diethyl ether at Ar atmosphere under anhydrous and dark conditions to afford $Pd(pph_3)_4$ (1.12 g, 86%).

1 or **2** (2.4 eq.), corresponding bromine **6**, **8**, **9** or **10** (1 eq.), Pd $(pph_3)_4$ (6% eq.), and sodium carbonate (120 eq.) were added to a mixed solvent (toluene:ethanol:water = 1:1:1.5, v/v/v) at Ar atmosphere. The reaction mixture was heated at 90 °C for 12 h in the dark. The reaction mixture was poured into water, extracted with ethyl acetate or dichloromethane, washed with water, dried with anhydrous sodium sulfate and filtered. The filtrate was concentrated under reduced pressure and the residue was purified by silica gel column chromatography or recrystallization to obtain the target compound.

Az-BT (0.52 g, 79%): M.p. 107–110 °C. ^{1}H NMR (400 MHz, $CDCl_3$, ppm) δ 8.69 (d, J = 4.0 Hz, 2H, ArH), 8.23 (d, J = 1.6 Hz, 2H, ArH), 7.69 (d, J = 4.0 Hz, 2H, ArH), 7.36 (dd, J = 10.8 Hz, 1.6 Hz, 2H, ArH), 7.26 (s, 2H, ArH), 7.05 (d, J = 10.8 Hz, 2H, ArH), 4.24 (t, J = 7.2 Hz, 4H, CH_2), 3.16-3.06 (m, 2H, CH), 2.92 (s, 6H, CH_3), 2.87 (s, 6H, CH_3), 2.10-2.03 (m, 4H, CH_2), 1.58-1.51 (m, 4H, CH_2), 1.40 (d, J = 7.2 Hz, 12H, CH_3), 1.37-1.23 (m, 16H, CH_2), 0.87 (t, J = 6.8 Hz, 6H, CH_3). ^{13}C NMR (100 MHz, $CDCl_3$, ppm) δ 151.9, 151.1, 143.5, 142.8, 141.5, 140.1, 138.4, 137.0, 135.3, 134.2, 133.0, 132.0, 126.7, 126.3, 121.1, 117.7, 112.5, 74.7, 38.6, 32.0, 30.7, 29.8, 29.5, 26.2, 24.9, 24.4, 22.8, 14.2, 12.6. Anal. calcd for $C_{60}H_{72}N_2O_2S_3$: C, 75.90; H, 7.64; N, 2.95; S, 10.13. Found: C, 75.49; H, 7.69; N, 3.12; S, 10.24.

Az-DPP (0.17 g, 48%): M.p. 268–269 °C. ^{1}H NMR (400 MHz, $CDCl_3$, ppm) δ 9.15 (d, J = 4.4 Hz, 2H, ArH), 8.23 (d, J = 1.6 Hz, 2H, ArH), 7.70 (d, J = 4.0 Hz, 2H, ArH), 7.50 (s, 2H, ArH), 7.38 (dd, J = 10.4 Hz, 1.6 Hz, 2H, ArH), 7.06 (d, J = 10.8 Hz, 2H, ArH), 4.20 (t, J = 7.6 Hz, 4H, CH_2), 3.15-3.04 (m, 2H, CH), 2.86 (s, 6H, CH_3), 2.85 (s, 6H, CH_3), 1.89-1.82 (m, 4H, CH_2), 1.54-1.47 (m, 4H, CH_2), 1.38 (d, J = 6.8 Hz, 12H, CH_3), 1.34-1.25 (m, 16H, CH_2), 0.86 (t, J = 6.8 Hz, 6H, CH_3). ^{13}C NMR spectrum was not characterized due to its poor solubility. Anal. calcd for $C_{60}H_{72}N_2O_2S_2$: C, 78.56; H, 7.91; N, 3.05; S, 6.99. Found: C, 78.25; H, 7.95; N, 3.33; S, 7.09.

Az-IID (0.23 g, 45%): M.p. 214–216 °C. ^{1}H NMR (400 MHz, $CDCl_3$, ppm) δ 9.19 (d, J = 8.4 Hz, 2H, ArH), 8.20 (d, J = 1.2 Hz, 2H, ArH), 7.51 (dd, J = 7.6 Hz, 3.6 Hz, 4H, ArH), 7.37-7.34 (m, 4H, ArH), 7.04 (d, J = 10.8 Hz, 2H, ArH), 6.99 (d, J = 1.2 Hz, 2H, ArH), 3.84 (t, J = 7.2 Hz, 4H, CH_2), 3.15-3.04 (m, 2H, CH), 2.85 (s, 6H, CH_3), 2.84 (s, 6H, CH_3), 1.80-1.73 (m, 4H, CH_2), 1.49-1.42 (m, 4H, CH_2), 1.39 (d, J = 7.2 Hz, 12H, CH_3), 1.36-1.22 (m, 16H, CH_2), 0.87 (t, J = 7.2 Hz, 6H, CH_3). ^{13}C NMR (100 MHz, $CDCl_3$, ppm) δ 168.4, 145.4, 144.4, 143.9, 142.3, 141.6, 139.5, 138.4, 137.8, 137.1, 134.5, 133.3, 131.8, 130.5, 127.8, 126.4, 125.6, 121.3, 121.1, 119.2, 112.3, 104.5, 40.2, 38.6, 32.0, 29.5, 29.4, 27.8, 27.2, 24.9, 24.5, 22.8, 14.2, 12.5. Anal. calcd for $C_{70}H_{78}N_2O_2S_2$: C, 80.57; H, 7.53; N, 2.68; S, 6.15. Found: C, 79.92; H, 7.55; N, 2.90; S, 6.19.

Az-TT (0.20 g, 77%): M.p. 165–166 °C. ^{1}H NMR (400 MHz, $CDCl_3$, ppm) δ 8.20 (s, 2H, ArH), 7.53 (s, 1H, ArH), 7.52 (s, 2H, ArH), 7.45 (s, 2H, ArH), 7.36 (d, J = 10.4 Hz, 2H, ArH), 7.31 (t, J = 4.0 Hz, 1H, ArH), 7.04 (d, J = 10.4 Hz, 2H, ArH), 4.29 (t, J = 5.6 Hz, 2H, CH_2), 3.14-3.04 (m, 2H, CH), 2.84 (t, J = 4.0 Hz, 12H, CH_3), 1.78-1.72 (m, 1H, CH), 1.51-1.46 (m, 2H, CH_2), 1.39 (d, J = 6.8 Hz, 12H, CH_3), 1.45-1.31 (m, 6H, CH_2), 1.00-0.93 (m, 6H, CH_3). ^{13}C NMR (100 MHz, $CDCl_3$, ppm) δ 161.6, 152.0, 149.1, 143.9, 143.8, 142.9, 141.6, 141.5, 139.02, 138.98, 138.4, 137.07, 137.04, 135.0, 134.44, 134.36, 134.3, 133.2, 133.1, 130.65, 130.56, 129.9, 129.7, 128.4, 128.3, 127.8, 127.5, 126.4, 125.1, 123.0, 121.1, 120.9, 112.15, 112.08, 68.2, 38.9, 38.6, 30.5, 29.1, 24.9, 24.5, 24.0, 23.1, 14.3, 12.5, 11.2. Anal. calcd for $C_{53}H_{55}FO_2S_4$: C, 73.06; H, 6.36; S, 14.72. Found: C, 73.55; H, 6.47; S, 15.82.

Na-BT (0.32 g, 81%): M.p. 138–139 °C. ^{1}H NMR (400 MHz, $CDCl_3$, ppm) δ 8.57 (d, J = 4.0 Hz, 2H, ArH), 8.18 (s, 2H, ArH), 7.90-7.84 (m, 8H, ArH), 7.58 (d, J = 4.0 Hz, 2H, ArH), 7.53-7.46 (m, 4H, ArH), 4.22 (t, J = 7.2 Hz, 4H, CH_2), 2.06-1.99 (m, 4H, CH_2), 1.58-1.50 (m, 5H, CH_2), 1.43-1.27 (m, 15H, CH_2), 0.86 (t, J = 6.8 Hz, 6H, CH_3). ^{13}C NMR (100 MHz, $CDCl_3$, ppm) δ 152.0, 151.0, 145.7, 134.1, 133.8, 133.0, 132.1, 131.9, 128.7, 128.2, 127.9, 126.7, 126.1, 124.4, 124.3, 123.6, 117.6, 74.7, 32.0, 30.7, 29.8, 29.5, 26.3, 22.8, 14.2. Anal. calcd for $C_{50}H_{52}N_2O_2S_3$: C, 74.22; H, 6.48; N, 3.46; S, 11.89. Found: C, 74.35; H, 6.48; N, 3.58; S 12.6.

Na-DPP (0.22 g, 58%): M.p. > 280 °C, ^{1}H NMR and ^{13}C NMR spectra were not characterized due to its very poor solubility. Anal. calcd for $C_{50}H_{52}N_2O_2S_2$: C, 77.28; H, 6.75; N, 3.60; S, 8.25. Found: C, 75.59; H, 6.65; N, 3.83; S, 8.47.

Na-IID (0.29 g, 65%): M.p. 253–254 °C, ^{1}H NMR (400 MHz, $CDCl_3$, ppm) δ 9.19 (d, J = 8.4 Hz, 2H, ArH), 8.08 (s, 2H, ArH), 7.87-7.76 (m, 8H, ArH), 7.52-7.39 (m, 8H, ArH), 7.33 (d, J = 8.4 Hz, 2H, ArH), 6.97 (s, 2H, ArH), 3.84 (t, J = 6.8 Hz, 4H, CH_2), 1.80-1.72 (m, 4H, CH_2), 1.50-1.22 (m, 20H, CH_2), 0.88 (t, J = 6.8 Hz, 6H, CH_3). ^{13}C NMR spectrum was not characterized due to its poor solubility. Anal. calcd for $C_{60}H_{58}N_2O_2S_2$: C, 79.78; H, 6.47; N, 3.10; S, 7.10. Found: C, 78.93; H, 6.46; N, 3.32; S, 7.27.

Na-TT (0.29 g, 81%): M.p. 181–182 °C. ^{1}H NMR (400 MHz, $CDCl_3$, ppm) δ 8.01 (s, 2H, ArH), 7.83-7.80 (m, 6H, ArH), 7.70 (d, J = 8.4 Hz, 2H, ArH), 7.49-7.36 (m, 7H, ArH), 7.17 (s, 1H, ArH), 4.25 (d, J = 6.0 Hz, 2H, CH_2), 1.77-1.71 (m, 1H, CH), 1.50-1.35 (m, 8H, CH_2), 0.99 (t, J = 7.6 Hz, 3H, CH_3), 0.97 (t, J = 7.2 Hz, 3H, CH_3). ^{13}C NMR (100 MHz, $CDCl_3$, ppm) δ 161.5, 149.1, 145.9, 144.5, 134.0, 133.7, 133.2, 133.05, 133.97, 131.0, 130.6, 130.5, 129.1, 128.8, 128.5, 128.23, 128.19, 127.9, 126.8, 126.4, 126.3, 125.2, 124.8, 124.4, 124.3, 124.1, 123.9, 123.8, 117.1, 68.3, 38.9, 30.6, 29.1, 24.0, 23.2, 14.3, 11.2. Anal. calcd for $C_{43}H_{35}FO_2S_4$: C, 70.65; H, 4.83; S, 17.54. Found: C, 68.72; H, 5.54; S 12.33.

3. Results and discussion

3.1. Synthesis and characterization

The synthetic routes of target compounds are outlined in Scheme 2. Guaiazulene borate (**1**) was synthesized by introduction of a boryl group into the 2-position of the guaiazulene skeleton through the direct C–H activation method with chloro(1,5-cyclooctadiene)iridium(I) dimer catalysis [29]. After heated at 80 °C for 20 h, about 45% of guaiazulene remained unreacted, which is consistent with the reported result [29]. Naphthalene borate (**2**) was synthesized by Miyaura boronation reaction of 2-bromo naphthalene with bis(pinacolato)diboron in a yield of 49% [30]. All target compounds were obtained by Suzuki coupling reaction of guaiazulene borate (**1**) or naphthalene borate (**2**) with the corresponding brominated intermediates (**6**, **8**, **9**, **10**) in yields of 45% ~

81%. The chemical structures of target compounds were confirmed by ^{1}H NMR, ^{13}C NMR and elemental analysis. The ^{13}C NMR spectra of Az-DPP, Na-IID and the ^{1}H NMR/^{13}C NMR spectra of Na-DPP weren't characterized due to their limited solubility. At room temperature, the solubility of Az-BT, Az-TT and Na-BT in chloroform solution is > 15 mg mL^{-1}, and the solubility of Az-IID and Na-TT is ~10 mg mL^{-1}. The solubility of Az-DPP and Na-IID is about 3–4 mg mL^{-1}, while that of Na-DPP is < 0.5 mg mL^{-1}. The solubility of azulene derivatives is generally higher than its corresponding naphthalene derivatives, which is mainly attributed to the alkyl substitutions in the guaiazulene structure.

3.2. Optical properties

The UV–visible absorption spectra of azulene and naphthalene derivatives in chloroform solution (1.0×10^{-5} mol L^{-1}) and thin films are shown in Fig. 3. The corresponding optical data are summarized in Table 1. In chloroform solution, all of these derivatives show multiple absorption peaks in the range of 200–750 nm, and the molar extinction coefficient (ε) of each peak wavelength is > 10^4 L mol^{-1} cm^{-1}. In all cases, azulene derivatives exhibit 10–39 nm red-shifted absorption spectra in the red visible region with respect to the corresponding naphthalene derivatives containing the same acceptor group, indicating a reduced energy gap of azulene derivatives due to the stronger electron-donating ability of the azulene group than that of naphthalene group [14,33,34]. The absorption spectra of azulene and naphthalene derivatives were also compared with guaiazulene (Az) or naphthalene (Na) and the corresponding parent electron-withdrawing units (**6**, **8**, **9** or **10**) in Fig. S1, evaluating the efficiency of conjugation through the backbone. Undoubtedly, azulene and naphthalene derivatives exhibit red-shifted absorption spectra with respect to the corresponding parent Az/Na and electron-withdrawing units, indicating the increased π-electron delocalization.

Table 1
Optical data of the target compounds.

compound	solution	film	
	λ_{max} (nm) (ε, × 10^4 L mol^{-1} cm^{-1})	λ_{max} (nm)	λ_{onset} (nm) (E_g^{opt}, eV)[a]
Az-BT	322 (4.08), 345 (4.21), 514 (3.73)	329, 541	667 (1.86)
Na-BT	248 (3.60), 351 (3.51), 482 (2.49)	363, 499	599 (2.07)
Az-DPP	316 (2.74), 427 (1.25), 619 (3.19)	323, 446, 642	821 (1.51)
Na-DPP	245 (2.77), 350 (2.28), 571 (4.09), 609 (4.56)	/[b]	/[b]
Az-IID	335 (5.35), 451 (3.24), 598 (4.07)	336, 467, 602	757 (1.64)
Na-IID	245 (4.63), 348 (3.02), 469 (2.24), 578 (3.19)	373, 487, 612, 663	730 (1.70)
Az-TT	316 (5.02), 427 (1.45), 534 (4.42)	322, 570	718 (1.73)
Na-TT	258 (3.72), 359 (2.22), 495 (3.33)	219, 382, 519	649 (1.91)

[a] Obtained from the onset of UV–Vis absorption spectra in thin films.
[b] The solubility of Na-DPP in chloroform is too poor (<0.5 mg mL^{-1}) to prepare spin-casting thin film sample.

In thin films, all of azulene and naphthalene derivatives display broadened and red-shifted absorption spectra in the range of 200–850 nm. According to the onset of the absorption spectra in thin films, the optical band gaps (E_g^{opt}) of azulene and naphthalene derivatives can be estimated to be 1.86 eV (Az-BT), 2.07 eV (Na-BT), 1.51 eV (Az-DPP), 1.64 eV (Az-IID), 1.70 eV (Na-IID), 1.73 eV (Az-TT) and 1.91 eV (Na-TT). The absorption spectrum of Na-DPP in thin film wasn't measured due to its too poor solubility in chloroform (<0.5 mg mL^{-1}) to prepare

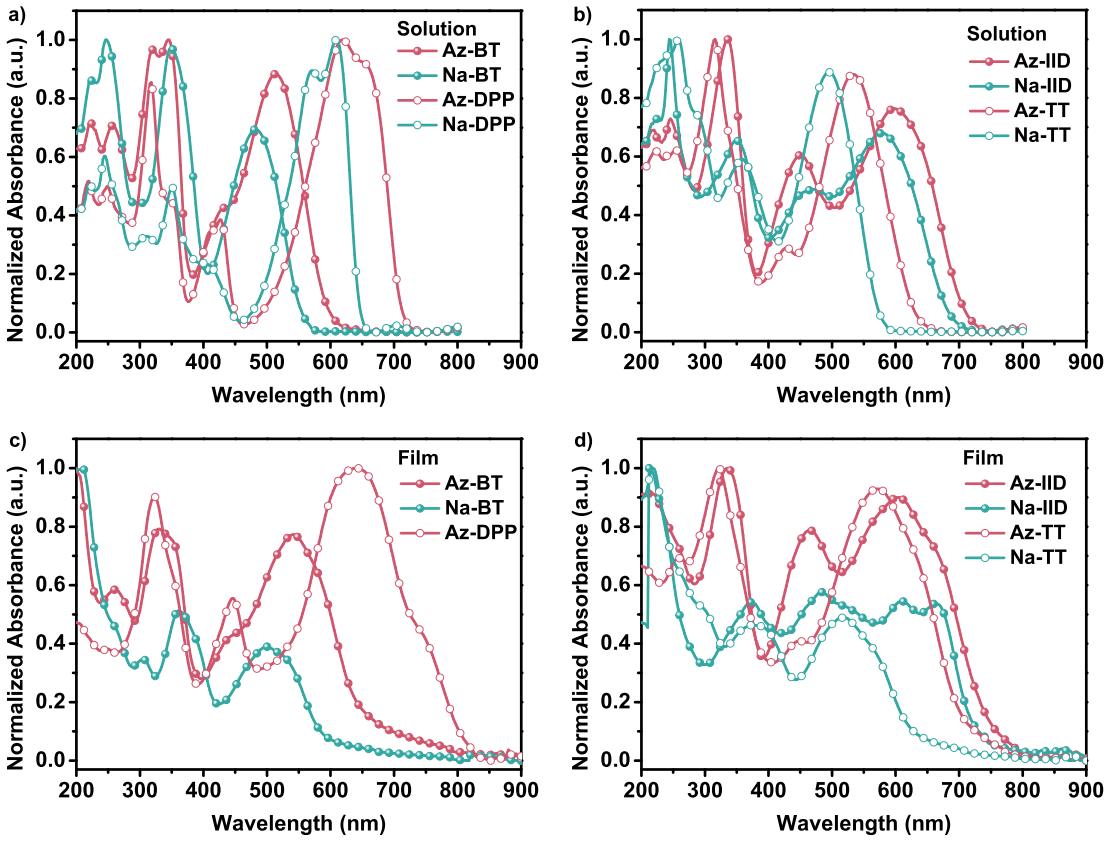

Fig. 3. UV–Visible absorption spectra of azulene and naphthalene derivatives in chloroform solution (a–b) and thin films (c–d).

spin-casting thin film.

3.3. Electrochemical properties

Cyclic voltammetry (CV) measurements were performed in CH_2Cl_2 to obtain the highest occupied molecular orbital (HOMO) and lowest unoccupied molecular orbital (LUMO) energy levels of these derivatives, shown in Fig. S2 and Table 2. In the anode scan, all of azulene derivatives and Na-DPP show an irreversible oxidation process in the range of 0.2–1 V while naphthalene derivatives (Na-BT, Na-IID and Na-TT) show a reversible oxidation process. According to the onset of the first oxidation wave *vs*. Fc/Fc^+ for these compounds and the energy level of Fc/Fc^+ redox couple (4.80 eV below vacuum) [7,35,36], the HOMO energy levels are calculated to be −5.16 eV for Az-BT, −5.36 eV for Na-BT, −5.03 eV for Az-DPP, −5.23 eV for Na-DPP, −5.16 eV for Az-IID, −5.35 eV for Na-IID, −5.07 eV for Az-TT and −5.23 eV for Na-TT. In the cathode scan, all of azulene and naphthalene derivatives except Na-DPP show an irreversible reduction process in the range of −1.6 ~ −1 V. According to the same calculation method of the HOMO energy level, the LUMO energy levels are calculated to be −3.39 eV for Az-BT, −3.38 eV for Na-BT, −3.33 eV for Az-DPP, −3.51 eV for Az-IID, −3.53 eV for Na-IID, −3.42 eV for Az-TT and −3.44 eV for Na-TT. It can be seen the HOMO energy levels of azulene derivatives are actually 0.16–0.2 eV higher than the corresponding naphthalene ones due to the stronger electron-donating ability of the azulene group, which is consistent with their absorption spectra. Meanwhile, the derivatives containing the same electron-withdrawing unit show the almost same LUMO energy levels. These results indicate that the HOMO energy level depends on the whole conjugated system, while the LUMO energy level mainly depends on the electron-withdrawing unit.

3.4. Photovoltaic properties

In order to research the effects of the azulene and naphthalene donor groups on the photovoltaic performance, solution processing OPVs based on azulene or naphthalene derivatives (electron donor material) and $PC_{71}BM$ (electron acceptor material) were fabricated. Unfortunately, the OPV devices based on Az-DPP and Na-DPP weren't prepared because of their rather poor solubility in chloroform. Initially, the photovoltaic performances of the devices based on Az-BT:$PC_{71}BM$ and Na-BT:$PC_{71}BM$ with different blend ratios were investigated. The relative *J-V* curves and photovoltaic data are shown in Table S1 and Fig. S3. For Az-BT-based devices, when the blend ratio is varied from 1:1 to 1:8, the PCE increases from 0.02% to 0.66%, along with simultaneously increased short circuit current density (J_{sc}), open circuit voltage (V_{oc}) and fill factor (FF). For Na-BT-based devices, when the blend ratio is from 1:1 to 1:5, the PCE increases significantly from 0.40% to 2.06%. Then the PCE decreases to 1.44% when the blend ratio is 1:8. It shows that the optimum blend ratio is found to be 1:8 for Az-BT-based devices and 1:5 for Na-BT-based ones. In order to compare the photovoltaic performances, the devices based on azulene and naphthalene derivatives with the blend ratio of 1:5 were prepared and discussed. The *J-V* curves and photovoltaic data are shown in Fig. 4 and Table 3.

Table 2
Electrochemical data and energy levels of the target compounds.

compounds	E_{ox}^{onset}(V)[a]	E_{red}^{onset}(V)[a]	HOMO (eV)[c]	LUMO (eV)[c]	E_g^{cv} (eV)[d]
Az-BT	0.36	−1.41	−5.16	−3.39	1.77
Na-BT	0.56[b]	−1.42	−5.36	−3.38	1.98
Az-DPP	0.23	−1.47	−5.03	−3.33	1.70
Na-DPP	0.43	/	−5.23	/	/
Az-IID	0.36	−1.29	−5.16	−3.51	1.65
Na-IID	0.55[b]	−1.27	−5.35	−3.53	1.82
Az-TT	0.27	−1.38	−5.07	−3.42	1.65
Na-TT	0.43[b]	−1.36	−5.23	−3.44	1.79

[a] Obtained from the onset of the first oxidation/reduction wave *vs*. Fc/Fc^+.
[b] Obtained from the peak of the first oxidation wave *vs*. Fc/Fc^+.
[c] HOMO = $(-4.80 - qE_{ox}^{onset})$ eV, LUMO = $(-4.80 - qE_{red}^{onset})$ eV.
[d] E_g^{CV} = LUMO − HOMO.

When the blend ratio is 1:5, azulene derivative-based devices exhibit moderate photovoltaic efficiencies (PCE = 0.26% ~ 0.57%) among the reported azulene-containing OPV materials (shown in Fig. 2) [13,20–23]. Meanwhile, in all cases, the devices based on naphthalene derivatives show relatively much higher PCEs (0.88% ~ 2.06%) than azulene derivatives-based ones, due to the higher J_{sc}, V_{oc} and FF. Az-BT- and Na-BT-based devices were taken as an example to discuss the effects of azulene and naphthalene groups on the photovoltaic performance. With respect to V_{oc}, the Na-BT-based device shows a V_{oc} of 1.04 V, which is 0.26 V higher than that of Az-BT-based one, consistent with the deeper of HOMO energy level by 0.2 eV. Further, the Na-BT-based device has a much higher J_{sc} of 6.01 mA cm^{-2} than that of Az-BT-based one (2.07 mA cm^{-2}), in good agreement with their EQE curves in Fig. 5a. In the entire region (300–800 nm), the EQE values of Na-BT-based device are significantly higher than that of Az-BT-based one. However, Az-BT- and Na-BT-based blend films exhibit quite similar absorption spectra, shown in Fig. 5b. Therefore, it might be rational to assign the difference of J_{sc} between these two devices to other factors rather than the absorption ability [36].

The hole mobility of Az-BT, Na-BT, Az-BT:$PC_{71}BM$ (1:5), and Na-BT:$PC_{71}BM$ (1:5) were measured and calculated by the space charge limited current (SCLC) model (Fig. 6) [27,28]. For pristine films, the hole mobility of Na-BT is calculated to be 2.31×10^{-5} cm^2 V^{-1} s^{-1}, which is about 14 times higher than that of Az-BT (1.64×10^{-6} cm^2 V^{-1} s^{-1}). For blend films, the hole mobility of Na-BT:$PC_{71}BM$ is 1.11×10^{-5} cm^2 V^{-1} s^{-1}, which is also much higher than that of Az-BT:$PC_{71}BM$ (6.84×10^{-7} cm^2 V^{-1} s^{-1}). The high hole mobility of photovoltaic devices is generally conducive to improve the charge transport, hence increase the corresponding J_{sc} and FF [37,38]. Therefore, the higher hole mobility of Na-BT-based devices than that of Az-BT-based ones contributes to the higher J_{sc} and FF in photovoltaic devices.

Furthermore, the film morphology of the blend films based on Az-BT:$PC_{71}BM$ (1:5) and Na-BT:$PC_{71}BM$ (1:5) were investigated by using AFM and TEM measurements. According to the AFM height graphics shown in Fig. 7a–b, the Na-BT:$PC_{71}BM$ blend film shows smoother surface with smaller root-mean-square (RMS) roughness (0.73 nm *vs*. 1.24 nm) than that of Az-BT:$PC_{71}BM$ blend film, which is beneficial to promote charge transfer [7]. For TEM results shown in Fig. 7c–d, Az-BT and Na-BT both exhibit good miscibility with $PC_{71}BM$ in the blend film, however, the phase separation size of Na-BT-based blend film is larger than that of

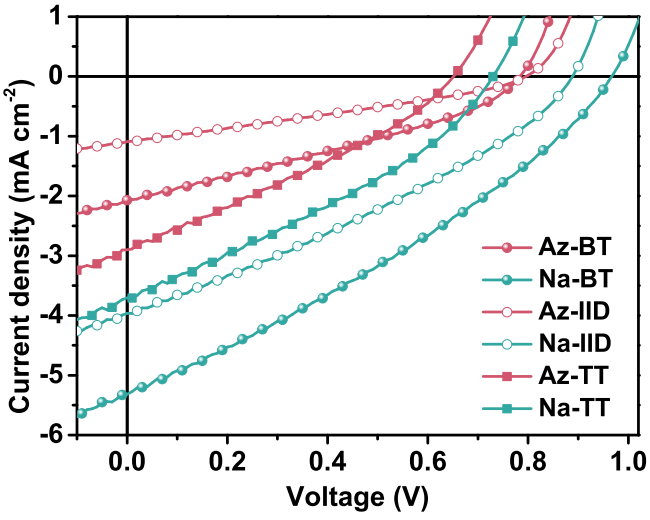

Fig. 4. The *J-V* curves of the devices based on azulene and naphthalene derivatives with the blend ratio of 1:5.

Table 3
Photovoltaic parameters of the devices based on azulene and naphthalene derivatives with the blend ratio of 1:5.[a]

Active layer	wt/wt	J_{sc} (mA cm^{-2})	V_{oc} (V)	FF	PCE (%)
Az-BT: $PC_{71}BM$	1:5	2.07 (1.56)	0.78 (0.72)	0.32 (0.30)	0.52 (0.35)
Na-BT: $PC_{71}BM$	1:5	6.01 (5.46)	1.04 (0.94)	0.33 (0.31)	2.06 (1.60)
Az-IID: $PC_{71}BM$	1:5	1.12 (1.10)	0.79 (0.79)	0.30 (0.29)	0.26 (0.26)
Na-IID: $PC_{71}BM$	1:5	3.97 (3.88)	0.89 (0.90)	0.32 (0.31)	1.12 (1.10)
Az-TT: $PC_{71}BM$	1:5	2.90 (2.72)	0.65 (0.58)	0.30 (0.30)	0.57 (0.48)
Na-TT: $PC_{71}BM$	1:5	3.71 (3.43)	0.73 (0.72)	0.33 (0.32)	0.88 (0.78)

[a] The average value of each photovoltaic parameter is shown in parentheses.

Az-BT-based one, promoting the charge transport after the exciton dissociation. Accordingly, the smoother surface topography and larger phase separation size of Na-BT-based blend film than those of Az-BT-based one also contribute to the higher J_{sc} and FF in photovoltaic devices. Additionally, the AFM and TEM measurements were also conducted on the blend films of Az-IID:$PC_{71}BM$, Na-IID:$PC_{71}BM$, Az-TT:$PC_{71}BM$, and Na-TT:$PC_{71}BM$, as shown in Fig. S4. With respect to AFM results, Na-IID and Na-TT blend films show rougher surface with larger RMS roughness (2.91 nm for Na-IID and 1.77 nm for Na-TT) than that of Az-IID and Az-TT blend films (1.20 nm for Az-IID and 1.07 nm for Az-TT). The rough surface morphology is not conducive to the effective contact between the active layer and the electrode, leading to the energy loss in photovoltaic devices [39]. Therefore, this is why the HOMO energy levels of Na-IID and Na-TT are 0.16–0.19 eV deeper than that of Az-IID and Az-TT, but the V_{oc} of Na-IID- and Na-TT-based devices are only 0.08–0.1 V higher than that of Az-IID- and Az-TT-based ones. With respect to TEM results, the phase separation size of Na-IID-based (or Na-TT-based) blend film is larger than that of Az-IID-based (Az-TT--based) one, contributing to the higher J_{sc} and FF in the corresponding photovoltaic devices.

As previously mentioned, although azulene derivatives show red-shifted and wider absorption spectra, naphthalene derivatives exhibit much lower HOMO energy levels, higher hole mobility, and better blend film morphology. Consequently, naphthalene derivatives show much more excellent photovoltaic performances (PCE = 0.88% ~ 2.06%), which is about 2–4 times higher than the corresponding azulene derivatives (PCE = 0.26% ~ 0.57%). In addition, with respect to the derivatives containing different electron-withdrawing units, Az-BT-based and Az-TT-based devices show rather similar PCEs (0.52% *vs.* 0.57%), which are approximately two times higher than Az-IID-based one

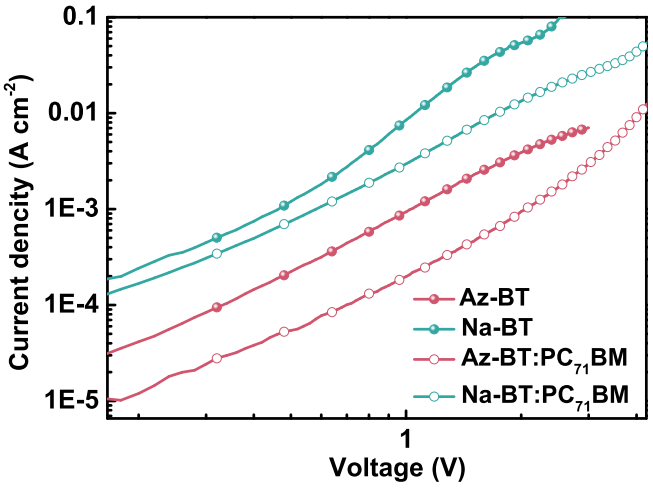

Fig. 6. *J-V* characteristics of hole-only single-carrier devices using Az-BT, Na-BT, Az-BT:$PC_{71}BM$ (1:5), and Na-BT:$PC_{71}BM$ (1:5) as active layer.

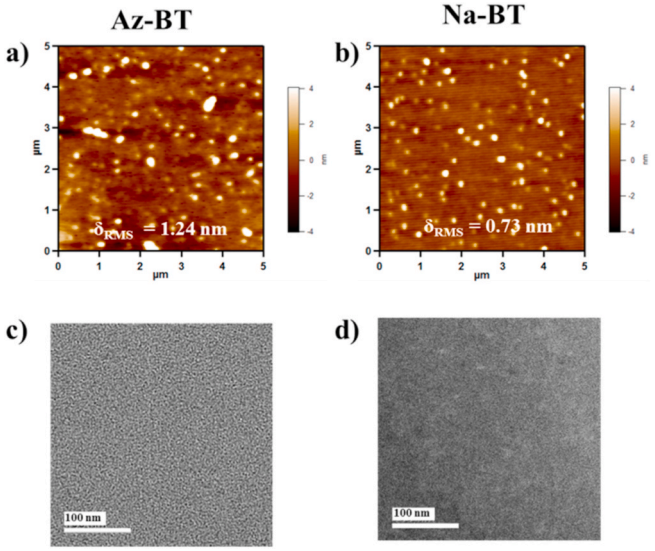

Fig. 7. The AFM height maps (a, b) and TEM images (c, d) of the blend films based on Az-BT:$PC_{71}BM$ (1:5, a, c) and Na-BT:$PC_{71}BM$ (1:5, b, d).

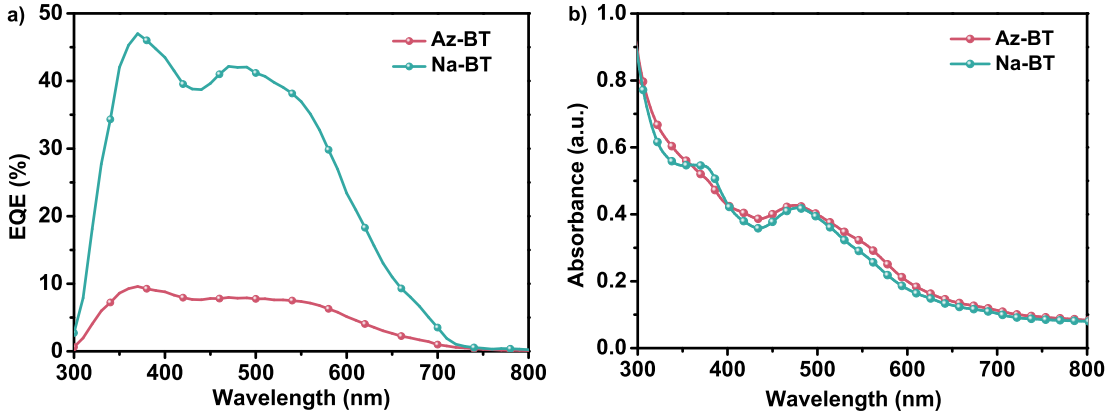

Fig. 5. The EQE curves of the devices (a) and the absorption spectra of the blend films (b) based on Az-BT and Na-BT with the blend ratio of 1:5.

(0.26%). Meanwhile, Na-BT-based device shows a PCE of 2.06%, which is also approximately two times higher than Na-IID- and Na-TT-based ones (PCE: 1.12% and 0.88% for Na-IID and Na-TT respectively). It can be seen that the derivatives containing BT unit have achieved the relatively high performance.

4. Conclusions

Eight D-A-D conjugated azulene and naphthalene derivatives, containing guaiazulene or naphthalene group as electron-donating moiety and BT, DPP, IID, or TT as electron-withdrawing moiety, were synthesized. The effects of azulene and naphthalene groups on the molecular properties and photovoltaic performances were investigated. The results show although azulene derivatives show red-shifted and wider absorption spectra, naphthalene derivatives exhibit much lower HOMO energy levels, higher hole mobility, and better film morphology. Unexpectedly, the devices based on naphthalene derivatives show relatively excellent PCE (0.88% ~ 2.06%), which is about 2–4 times higher than that of the corresponding azulene derivatives (PCE = 0.26% ~ 0.57%). Additionally, the derivatives containing BT unit have achieved the relatively better performance than the derivatives containing IID and TT units, indicating that selecting appropriate D and A units plays a particularly important role in the development of D-A conjugated photovoltaic materials.

Author statement

Lin Yang and Yan Huang conceived the idea and prepared the paper. Lin Yang synthesized most of the compounds, characterized the properties, analyzed the results and prepared the original draft. Youqin Zhu and Suling Zhao fabricated OPVs and performed the J-V performances, EQE, and SCLC measurements. Jueshan Liu, Yao Chen, Jianglin Wu, and Zhenguo Pang provided useful help in synthesis, testing and discussion. Lin Yang, Zhiyun Lu and Yan Huang supervised the project. All authors commented on the paper and have given approval to the final version of the manuscript.

Declaration of competing interest

The authors declare that they have no known competing financial interests or personal relationships that could have appeared to influence the work reported in this paper.

Acknowledgements

We acknowledge the financial support for this work from the National Natural Science Foundation of China (project No. 21875148, 51573108 and 21672156), the Science and Technology Strategic Cooperation Programs of Luzhou Municipal People's Government and Southwest Medical University (project No. 2019LZXNYDZ09) and School Foundation of Southwest Medical University (project No. 2018-ZRZD-002 and 2019ZZD012). We are grateful to the Comprehensive Training Platform of Specialized Laboratory, College of Chemistry, Sichuan University for providing NMR and elemental analyses.

Appendix A. Supplementary data

Supplementary data to this article can be found online at https://doi.org/10.1016/j.dyepig.2020.109079.

References

[1] Ni W, Wan X, Li M, Wang Y, Chen Y. A-D-A small molecules for solution-processed organic photovoltaic cells. Chem Commun 2015;51:4936–50.
[2] Cui Y, Yao H, Zhang J, Xian K, Zhang T, Hong L, et al. Single-junction organic photovoltaic cells with approaching 18% efficiency. Adv Mater 2020;32:1908205.
[3] Zhu C, Yuan J, Cai F, Meng L, Zhang H, Chen H, et al. Tuning the electron-deficient core of a non-fullerene acceptor to achieve over 17% efficiency in a single-junction organic solar cell. Energy Environ Sci 2020;13:2459–66.
[4] Zhan L, Li S, Lau TK, Cui Y, Lu X, Shi M, et al. Over 17% efficiency ternary organic solar cells enabled by two non-fullerene acceptors working in an alloy-like model. Energy Environ Sci 2020;13:635–45.
[5] Dey S. Recent progress in molecular design of fused ring electron acceptors for organic solar cells. Small 2019;15:1900134.
[6] Fu H, Wang Z, Sun Y. Polymer donors for high-performance non-fullerene organic solar cells. Angew Chem Int Ed 2019;58:4442–53.
[7] Ma X, Luo M, Gao W, Yuan J, An Q, Zhang M, et al. Achieving 14.11% efficiency of ternary polymer solar cells by simultaneously optimizing photon harvesting and exciton distribution. J Mater Chem A 2019;7:7843–51.
[8] Liu Q, Jiang Y, Jin K, Qin J, Xu J, Li W, et al. 18% Efficiency organic solar cells. Sci Bull 2020;65:272–5.
[9] Anderson AG, Steckler BM, Azulene VIII. A study of the visible absorption spectra and dipole moments of some 1- and 1,3-substituted azulenes. J Am Chem Soc 1959;81:4941–6.
[10] Xin H, Gao X. Application of azulene in constructing organic optoelectronic materials: new tricks for an old dog. ChemPlusChem 2017;82:945–56.
[11] Lemal DM, Goldman GD. Synthesis of azulene, a blue hydrocarbon. J Chem Educ 1988;65:923–5.
[12] Cowper P, Pockett A, Kociok-Kohn G, Cameron PJ, Lewis SE. Azulene-thiophene-cyanoacrylic acid dyes with donor-π-acceptor structures. Synthesis, characterization and evaluation in dye-sensitized solar cells. Tetrahedron 2018;74:2775–86.
[13] Xin H, Ge C, Jiao X, Yang X, Rundel K, McNeill CR, et al. Incorporation of 2,6-connected azulene units into the backbone of conjugated polymers: towards high-performance organic optoelectronic materials. Angew Chem Int Ed 2017;57:1322–6.
[14] Muranaka A, Yonehara M, Uchiyama M. Azulenocyanine: a new family of phthalocyanines with intense near-IR absorption. J Am Chem Soc 2010;132:7844–5.
[15] Xin H, Ge C, Fu L, Yang X, Gao X. Naphthalene diimides endcapped with ethynylazulene: molecular design, synthesis and properties. Chin J Org Chem 2017;37:711–9.
[16] Yamaguchi Y, Ogawa K, Nakayama K, Ohba Y, Katagiri H. Terazulene: a high-performance n-type organic field-effect transistor based on molecular orbital distribution control. J Am Chem Soc 2013;135:19095–8.
[17] Smits ECP, Setayesh S, Anthopoulos TD, Buechel M, Nijssen W, Coehoorn R, et al. Near-infrared light-emitting ambipolar organic field-effect transistors. Adv Mater 2007;19:734–8.
[18] Xin H, Li J, Yang X, Gao X. Azulene-based BN-heteroaromatics. J Org Chem 2020;85:70–8.
[19] Gao H, Ge C, Hou B, Xin H, Gao X. Incorporation of 1,3-free-2,6-connected azulene units into the backbone of conjugated polymers: improving proton responsiveness and electrical conductivity. ACS Macro Lett 2019;8:1360–4.
[20] Yao J, Cai Z, Liu Z, Yu C, Luo H, Yang Y, et al. Tuning the semiconducting behaviors of new alternating dithienyldiketopyrrolopyrrole-azulene conjugated polymers by varying the linking positions of azulene. Macromolecules 2015;48:2039–47.
[21] Umeyama T, Watanabe Y, Miyata T, Imahori H. Electron-rich five-membered ring of azulene as a donor unit in donor-acceptor alternating copolymers for polymer solar cell applications. Chem Lett 2015;44:47–9.
[22] Puodziukynaite E, Wang HW, Lawrence J, Wise AJ, Russell TP, Barnes MD, et al. Azulene methacrylate polymers: synthesis, electronic properties, and solar cell fabrication. J Am Chem Soc 2014;136:11043–9.
[23] Chen Y, Zhu Y, Yang D, Zhao S, Zhang L, Yang L, et al. An azulene-containing low bandgap small molecule for organic photovoltaics with high open-circuit voltage. Chem Eur J 2016;22:14527–30.
[24] Zhang XH, Li C, Wang WB, Cheng XX, Wang XS, Zhang BW. Photophysical, electrochemical, and photoelectrochemical properties of new azulene-based dye molecules. J Mater Chem 2007;17:642–9.
[25] Nishimura H, Ishida N, Shimazaki A, Wakamiya A, Saeki A, Scott LT, et al. Hole-transporting materials with a two-dimensionally expanded π-System around an azulene core for efficient perovskite solar cells. J Am Chem Soc 2015;137:15656–9.
[26] Truong MA, Lee J, Nakamura T, Seo JY, Jung M, Ozaki M, et al. Influence of alkoxy chain length on the properties of two-dimensionally expanded azulene-core-based hole-transporting materials for efficient perovskite solar cells. Chem Eur J 2019;25:6647–752.
[27] Azimi H, Senes A, Scharber MC, Hingerl K, Brabec CJ. Charge transport and recombination in low-bandgap bulk heterojunction solar cell using bis-adduct fullerene. Adv Energy Mater 2011;1:1162–8.
[28] Zhu Y, Yang L, Zhao S, Huang Y, Xu Z, Yang Q, et al. Improved performances of PCDTBT:$PC_{71}BM$ BHJ solar cells through incorporating small molecule donor. Phys Chem Chem Phys 2015;17:26777–82.
[29] Kurotobi K, Miyauchi M, Takakura K, Murafuji T, Sugihara Y. Direct introduction of a boryl substituent into the 2-position of azulene: application of the miyaura and smith methods to azulene. Eur J Org Chem 2003;2003:3663–5.
[30] Kim KS, Jeong S, Kim C, Ham JY, Kwon Y, Choi BD, et al. Synthesis and electro-optical properties of carbazole derivatives for organic device applications. Synthetic Met 2009;159:1870–5.
[31] Mei J, Graham KR, Stalder R, Reynolds JR. Synthesis of isoindigo-based oligothiophenes for molecular bulk heterojunction solar cells. Org Lett 2010;12:660–3.

[32] Zhang M, Guo X, Zhang S, Hou J. Synergistic effect of fluorination on molecular energy level modulation in highly efficient photovoltaic polymers. Adv Mater 2014;26:1118–23.
[33] Murai M, Ku SY, Treat ND, Robb MJ, Chabinyc ML, Hawker CJ. Modulating structure and properties in organic chromophores: influence of azulene as a building block. Chem Sci 2014;5:3753–60.
[34] Cristian L, Sasaki I, Lacroix PG, Donnadieu B, Asselberghs I, Clays K, et al. Donating strength of azulene in various azulen-1-yl-substituted cationic dyes: Application in nonlinear optics. Chem Mater 2004;16:3543–51.
[35] Kan B, Feng H, Wan X, Liu F, Ke X, Wang Y, et al. A small molecule acceptor based on the heptacyclic benzodi(cyclopentadithiophene) unit for high efficient non-fullerene organic solar cells. J Am Chem Soc 2017;139:4929–34.
[36] Yang L, Zhu Y, Jiao Y, Yang D, Chen Y, Wu J, et al. The influence of intramolecular noncovalent interactions in unsymmetrical squaraines on material properties, film morphology and photovoltaic performance. Dyes Pigments 2017;145:222–32.
[37] Jao MH, Liao HC, Su WF. Achieving a high fill factor for organic solar cells. J Mater Chem A 2016;4:5784–801.
[38] Yang L, Yang Q, Yang D, Luo Q, Zhu Y, Huang Y, et al. Marked effects of indolyl *vs.* indolinyl substituent on solid-state structure, carrier mobility and photovoltaic efficiency of asymmetrical squaraine dyes. J Mater Chem A 2014;2:18313–21.
[39] Tuladhar SM, Azzouzi M, Delval F, Yao J, Guilbert AAY, Kirchartz T, et al. Low open-circuit voltage loss in solution-processed small-molecule organic solar cells. ACS Energy Lett 2016;1:302–8.